2012

Structural control of d-f interaction in the CeFe1−xRuxAsO system system

Cao Wang
University of Wollongong, caow@uow.edu.au

Hao Jiang
Zhejiang University

Yongkang Luo
Zhejiang University

Chunmu Feng
Zhejiang University

Wenxian Li
University of Wollongong, wenxian@uow.edu.au

See next page for additional authors

Publication Details

Wang, C., Jiang, H., Luo, Y., Feng, C., Li, W., Xu, Z., Cao, G., Kim, J. & Dou, S. Xue. (2012). Structural control of d-f interaction in the CeFe1−xRuxAsO system system. Europhysics Letters: a letters journal exploring the frontiers of physics, 99 (5), 57009-p1-57009-p6.

A Letters Journal Exploring the Frontiers of Physics

September 2012

EPL, **99** (2012) 57009
doi: 10.1209/0295-5075/99/57009

www.epljournal.org

Structural control of d-f interaction in the $CeFe_{1-x}Ru_xAsO$ system

Cao Wang[1,2], Hao Jiang[2], Yongkang Luo[2], Chunmu Feng[2], Wenxian Li[1], Zhu'an Xu[2], Guanghan Cao[2], Jung Ho Kim[1(a)] and Shixue Dou[1(b)]

[1] *Institute for Superconducting and Electronic Materials, University of Wollongong North Wollongong, NSW 2522, Australia*
[2] *Department of Physics, Zhejiang University - Hangzhou 310027, China*

received 20 June 2012; accepted in final form 9 August 2012
published online 13 September 2012

PACS 74.70.Xa – Pnictides and chalcogenides
PACS 75.20.Hr – Local moment in compounds and alloys; Kondo effect, valence fluctuations, heavy fermions
PACS 71.20.Eh – Rare earth metals and alloys

Abstract – The isovalent substitution effect of Ru in $CeFe_{1-x}Ru_xAsO$ ($0 \leqslant x \leqslant 1$) has been systematically studied by powder X-ray diffraction, electrical resistivity, magnetization, and specific heat measurements. The antiferromagnetic (AFM) ordering of both d and $4f$ electrons are suppressed upon Ru doping, followed by Pauli paramagnetism (d electrons) and local moment paramagnetism ($4f$ electrons) with strong ferromagnetic fluctuation, respectively. Neither superconductivity above 2 K nor pronounced Kondo screening are observed in the substitution phase diagram. Combined with published results of the cerium-based quaternary compounds $CeMXO$($M =$ Fe, Ru; $X =$ P, As), our data suggest that the end member CeRuAsO is on the verge of becoming an FM Kondo lattice. Meanwhile, the ground state of $4f$ electrons in the quaternary $CeMXO$ system should be determined by both the interlayer d-f Kondo coupling (J_{Kondo}) and the intralayer Ruderman-Kittel-Kasuya-Yosida (RKKY) interaction (J_{RKKY}), which are both very sensitive to the change in crystal structure.

Introduction. – The discovery of 26 K superconductivity in $LaFeAsO_{1-x}F_x$ [1] aroused broad interest in the iron-based ZrCuSiAs-type compounds. It is now clear that both electron [1–3] and hole doping [4] can induce superconductivity in LaFeAsO. Generally, the superconducting transition temperature (T_c) exceeds the McMillan limit when La is replaced by other heavier rare-earth elements [2,5–10]. As to the isovalent substitution (say phosphorus for arsenic) in the so-called "1111" phases, however, the rule of thumb above does not work any more. While P doping induces unconventional superconductivity in $LaFeAs_{1-x}P_xO$ with T_c of 10 K [11], the superconducting T_c of the $SmFeAs_{1-x}P_xO$ system is only 4.1 K [12].

Aside from P (for As), Ru (for Fe) is another isovalent substitution which is supposed not to introduce extra carriers. Summarizing the experiments on these two isovalent dopants in "1111" phases, one can easily find the difference: Firstly, nearly twice as much Ru content as that of P substitution is required to destroy the antiferromagnetic (AFM) state of d electrons [11,13]. Secondly, no superconductivity higher than 2 K has been reported with Ru substitution so far. In the "122" phases, however, both P and Ru substitution can achieve high-T_c superconductivity with similar optimal doping level and T_c [14–19]. It is rather remarkable that the superconductivity observed in P doped "1111" phases is theoretically ascribed to quantum critical behavior [20], which is induced by the enhanced itinerancy of d electrons [21,22]. Interestingly, recent experimental work showed that the substitution of Ru for Fe in $BaFe_{2-x}Ru_xAs_2$ can also enhance the itinerancy of d electrons [23,24].

Among the $LnMXO$ ($Ln =$ lanthanide; $M =$ Fe, Ru; $X =$ P, As) system, the Ce-based compounds are unique for studying the interaction between the d and f electrons. While CeFeAsO is an itinerant AFM bad metal with localized Ce $4f$ electrons that undergo AFM ordering below 4 K [6,25], CeFePO acts as a paramagnetic (PM) heavy-fermion metal with ferromagnetic (FM) fluctuation [26]. For Ru-based "1111" compounds, CeRuPO has been reported as a rare example of an FM Kondo lattice [27], yet the physical properties of CeRuAsO are still unclear, except for the metallic resistivity down to 4 K [28]. The substitution phase diagram between

(a) E-mail: jhk@uow.edu.au
(b) E-mail: shi_dou@uow.edu.au

CeFeAsO and CeFePO shows that, the ordering of Ce $4f$ electrons changes from AFM to FM at the P doping level of $x = 0.37$, combined with the the disappearance of Fe^{2+} long-range AFM order. For the range of $x \geqslant 0.95$, the localized $4f$ electrons are screened by the spin of the conduction sea, resulting in heavy-fermion behaviors [29]. Thus, considering the the similarity between Ru and P substitution and the rich physics relating to d-f coupling in the Ce-based "1111" compounds, it is interesting to know the Ru doping effects in CeFeAsO system.

In this paper, the evolution of physical properties in $CeFe_{1-x}Ru_xAsO$ ($0 \leqslant x \leqslant 1$) has been systematically studied by X-ray powder diffraction (XRD), electric resistivity, magnetic susceptibility, isothermal magnetization and specific heat. Our results show that, while Ru substitution gradually suppressed the AFM state of d electrons, just like what it did in other iron-based "1111" compounds, the AFM of $4f$ local moment vanishes simultaneously followed by strong FM fluctuation, which was not observed in its analogue $PrFe_{1-x}Ru_xAsO$ system [30]. Compared with $CeFeAs_{1-x}P_xO$ on the other hand, no pronounced heavy-fermion behavior is observed. Combined with other published works about $CeMXO$ ($M =$ Fe, Ru; $X =$ P, As) compounds, we suggest that the ground state of cerium $4f$ orbital is dependent on both the vertical distance between Ce and Fe/Ru planar layers ($D_{\text{Ce-Fe/Ru}}$) and the distance between the nearest Ce atoms ($D_{\text{Ce-Ce}}$).

Experimental. – Polycrystalline samples of $CeFe_{1-x}Ru_xAsO$ were synthesized using a solid-state reaction in an evacuated quartz tube. All the starting materials, including Ce, Ru, Fe, As, and CeO_2 have high purity ($\geqslant 99.9\%$). CeAs was presynthesized by reacting stoichiometric Ce powder and As powder in vacuum at 350 °C for 10 hours and then at 700 °C for 12 hours. Similarly, RuAs and FeAs were prepared by reacting Ru/Fe powder and As powder at 500 °C and then at 700 °C. Then powders of CeAs, CeO_2, RuAs, FeAs, Fe and Ru were weighed according to the stoichiometric ratio of $CeFe_{1-x}Ru_xAsO$. The weighed powders were mixed thoroughly by grinding, and pressed into pellets under a pressure of 4000 kg cm^{-2}. All the reagents were handled in a glove box under high purity argon atmosphere. The pellet was put into a small crucible and sealed in an evacuated quartz ampoule. The sealed ampoule was slowly heated to 1150 °C, held at that temperature for 50 hours and finally furnace-cooled to room temperature. The solid-state reaction was repeated with intermediate regrinding.

Powder X-ray diffraction (XRD) was performed at room temperature using a D/Max-rA diffractometer with Cu K_α radiation and a graphite monochromator. The XRD diffractometer system was calibrated using standard Si powders. Lattice parameters were calculated by a least-squares fit using at least 20 XRD peaks in the range of $20° \leqslant 2\theta \leqslant 80°$. Crystal structure details were obtained by Rietveld refinement using the step-scan XRD data with

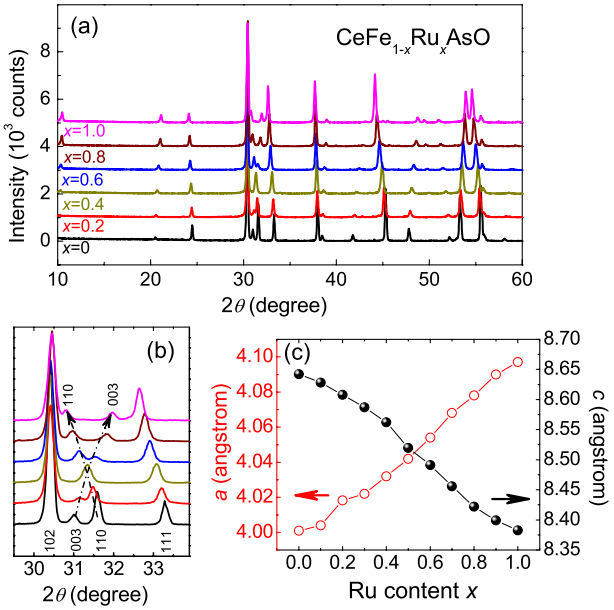

Fig. 1: (Color online) (a) Powder X-ray diffraction patterns of $CeFe_{1-x}Ru_xAsO$ samples. (b) Magnified XRD patterns indicating the peak shift with the Ru substitution. (c) Lattice parameters as functions of different Ru content in the $CeFe_{1-x}Ru_xAsO$ system.

$20° \leqslant 2\theta \leqslant 120°$ for all the samples. The refined lattice constants are essentially the same as those from the least-squares fit within the scope of estimated errors. The typical R-factors of the refinements are: $R_F \sim 2\%$, $R_B \sim 3\%$, and $R_{wp} \sim 11\%$. The goodness-of-fit parameter, $S = R_{wp}/R_{exp} \sim 1.5$, indicating good reliability of the refinement [31]. The electrical resistivity was measured with the standard four-terminal method, after checking the linear I-V characteristic. Magnetic susceptibility and isothermal magnetization measurements were performed on a Quantum Design magnetic property measurement system (MPMS-5). Specific-heat measurements were carried out on a Quantum Design physical property measurement system (PPMS-14).

Results and discussion. – Figure 1(a) shows the XRD patterns of the synthesized $CeFe_{1-x}Ru_xAsO$ samples. The XRD peaks can be well indexed based on a tetragonal cell of CeFeAsO with space group $P4/nmm$ (No. 129). No obvious impurity peak is found, suggesting that Ru is successfully doped into the lattice. As is shown in fig. 1(b), while the (003) peak shifts to higher angle the (110) peak shifts to lower one, indicating the expansion and shrinkage of a-axis and c-axis, respectively. This observation is consistent with the calculated lattice parameters as functions of nominal Ru content, which are shown in fig. 1(c). We note that such an anisotropic structural evolution were also observed in $4d/5d$ transition metal substitution experiments in other "1111" phases [13,30,32–34].

Table 1: Comparison of structure details in CeFePO, CeRuPO, CeRuAsO and CeFeAsO. The space group is $P4/nmm$. The atomic coordinates (x, y, z) are as follows: Ce $(\frac{1}{4}, \frac{1}{4}, z)$; O $(\frac{3}{4}, \frac{1}{4}, 0)$; Fe/Ru $(\frac{3}{4}, \frac{1}{4}, \frac{1}{2})$; As/P $(\frac{1}{4}, \frac{1}{4}, z)$. $H_{Ce_2O_2}$ and $H_{Fe_2As_2}$ represent the thickness of the Ce_2O_2 and Fe_2As_2 layers respectively. $D_{\text{Ce -Fe/Ru}}$ indicates the vertical distance between the planar layers of Ce and Fe/Ru.

Systems	CeFePO [26,29]	CeRuPO [35]	CeRuAsO	CeFeAsO
a (Å)	3.919(3)	4.026(1)	4.098(2)	4.002(1)
c (Å)	8.330(5)	8.256(2)	8.386(4)	8.646(3)
z of Ce	0.1508	0.1472	0.1408	0.1411
z of As/P	0.6384	0.6419	0.6546	0.6547
$H_{Ce_2O_2}$ (Å)	2.512	2.431	2.356	2.440
$H_{Fe_2As_2}$ (Å)	2.306	2.343	2.593	2.675
$D_{\text{Ce-Fe/Ru}}$ (Å)	2.901	2.913	3.014	3.103

Based on Rietveld refinement and some other published works, table 1 summarizes the structural data on CeFePO, CeRuPO, CeRuAsO and CeFeAsO. From the table we can find that: i) Compared with P substitution which results in a thickened Ce_2O_2 layer and a compressed $Fe_2As(P)_2$ layer, the "chemical pressure" along the c-axes induced by Ru substitution is exerted uniformly on both Ce_2O_2 and $(Fe/Ru)_2As_2$ layers. We note that a similar phenomenon was also observed in $PrFe_{1-x}Ru_xAsO$ [30]. This may explain the absence of superconductivity in Ru-doped "1111" phases as a selective chemical pressure on the Fe_2As_2 layer rather than a uniform one on both layers is required [11]. ii) The $D_{\text{Ce-Fe/Ru}}$ shrinks from 3.103 Å to 3.014 Å in $CeFe_{1-x}Ru_xAsO$ while that of the $CeFeAs_{1-x}P_xO$ decreases from 3.103 Å to 2.901 Å. So the maximum shrinkage of $D_{\text{Ce-Fe/Ru}}$ in $CeFe_{1-x}Ru_xAsO$ ($x = 1$) is equivalent to that of $x = 0.45$ in the $CeFeAs_{1-x}P_xO$ system. As far as the relationship between d-f coupling and $D_{\text{Ce-Fe/Ru}}$ is concerned [29,36], these structural characteristics are consistent with the absence of heavy-fermion behavior in $CeFe_{1-x}Ru_xAsO$ (as will be discussed later).

Figure 2 shows the temperature dependence of electrical resistivity (ρ-T) of $CeFe_{1-x}Ru_xAsO$. Although no superconductivity is observed throughout the whole temperature range, the figure still provides important information: Firstly, an anomaly characterized by a drop in ρ was observed below 140 K for the end-member CeFeAsO, consistent with the previous reports [6]. This anomaly was ascribed to the structure distortion and the accompanying Fe-AFM transition [25]. Upon Ru doping, the anomaly is suppressed monotonically and cannot be identified clearly for $x > 0.6$. Meanwhile an upturn is observed at low temperature, which is most likely due to remnant AFM instability. Secondly, the room temperature resistivity decreases gradually from 21 mΩ cm (CeFeAsO) to 4 mΩ cm (CeRuAsO) upon Ru doping. Indeed the resistivity of polycrystalline sample may not reflect the intrinsic property due to the possible metallic impurities dwelling at grain-boundaries such as FeAs and RuAs. However, the monotonic decrease in room temperature resistivity does suggest the enhanced metallic behavior,

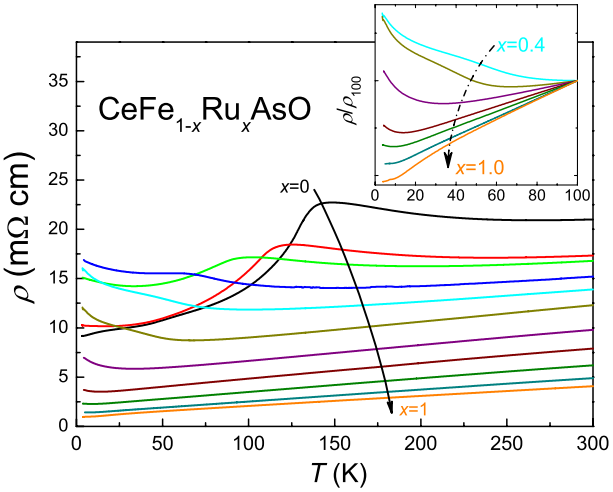

Fig. 2: (Color online) Temperature dependence of the electrical resistivity of $CeFe_{1-x}Ru_xAsO$. The inset shows the normalized resistivity in the range of $0.4 \leqslant x \leqslant 1$, where the AFM of Fe^{2+} and the consequent resistivity upturn are completely suppressed.

considering the high sample quality shown by the XRD profile. We note that a similar increased conductivity is also observed in $PrFe_{1-x}Ru_xAsO$. At the same time, both *ab initio* calculation [37] and NMR [38] measurement in the similar $LaFe_{1-x}Ru_xAsO$ system indicated that Ru for Fe substitution yields a progressive decrease of the density of states at the Fermi level. This suggest that Ru substitution in iron-based "1111" compounds may enhance the itineracy of d electrons.

The dc magnetic susceptibility was measured under a field of 1000 Oe (fig. 3). The susceptibility increases with decreasing temperature in the high-temperature region, following the Curie-Weiss law for all the samples of $0 \leqslant x \leqslant 1$. The effective moments μ_{eff} derived from the data above 200 K ranges from $2.50\mu_B$ to $2.61\mu_B$, which are very close to that of a free Ce^{3+} ion ($2.54\,\mu_B$). As the temperature drops, the $1/\chi - T$ relation for all the samples gradually deviates from linearity denoting the crystalline electric field effect. In the low-temperature region, the

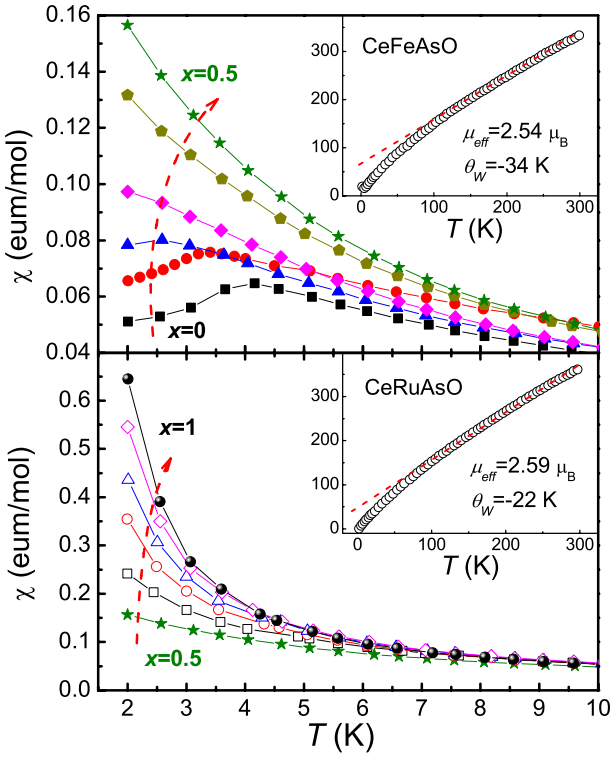

Fig. 3: (Color online) Temperature dependence of the *dc* magnetic susceptibility below 10 K for $CeFe_{1-x}Ru_xAsO$. The inset shows the $1/\chi$-T relations for end members CeFeAsO and CeRuAsO.

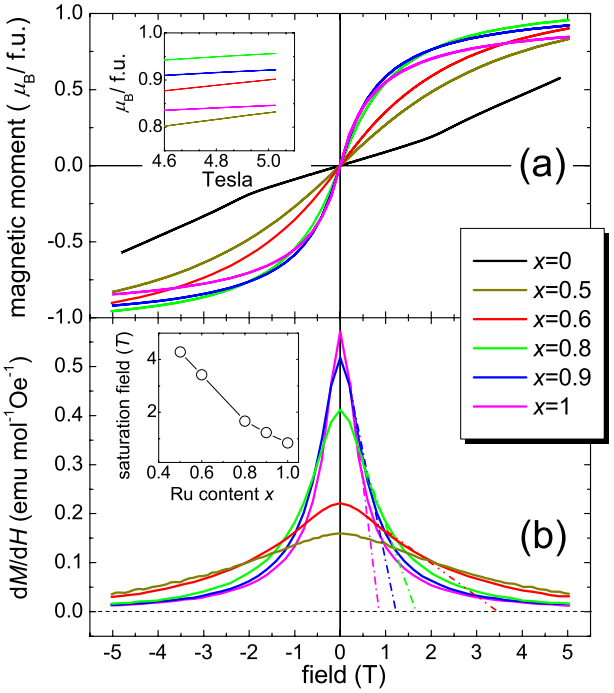

Fig. 4: (Color online) (a) Isothermal magnetization of $CeFe_{1-x}Ru_xAsO$ at 2 K. The inset shows the expanded M-H curves at high field for $x = 0.5$, 0.6, 0.8, 0.9, 1. (b) The derivative of magnetization with respect to magnetic field for $x = 0.5$, 0.6, 0.8, 0.9, 1. The inset shows the Ru content dependent ferromagnetic saturation field.

susceptibility of CeFeAsO exhibits a peak at 4.1 K, denoting the formation of the Ce^{3+} AFM order. Upon Ru doping, the AFM peak is suppressed to lower temperature and cannot be identified for $x \geqslant 0.4$, where an increasingly robust susceptibility upturn is observed. Although there is not any substantial divergence between zero-field-cooling (ZFC) and field-cooling (FC) curves, such a Ru content dependent susceptibility upturn does suggest the eve of FM transition, considering the good sample quality. We note that in the analog $PrFe_{1-x}Ru_xAsO$ system, the Néel temperature ($T_N f$) of Pr^{3+} AFM is Ru content independent [30]. This indicates that the $CeFe_{1-x}Ru_xAsO$ system is similar to $CeFeAs_{1-x}P_xO$ rather than $PrFe_{1-x}Ru_xAsO$ where the d-f orbital coupling can be safely disregarded.

The evolution of the $4f$ coupling can be further demonstrated by isothermal field-dependent magnetization measurements (fig. 4(a)). The temperature is fixed at 2 K. For the end member CeFeAsO, a kink in the magnetization curve is observed, consistent with Luo *et al.* [29]. Upon Ru doping, the kink disappears, while the magnetization curve begins to deviate from linearity and tends to saturate at high field, suggesting the enhanced FM interaction. No hysteresis loops were observed for any of the magnetization curves, which can be explained as the absence of long-range FM order. The maximum of saturated M appears at around $x = 0.8$ with a value of $0.96\,\mu_B$, close to the $1\,\mu_B$ expected for a Ce^{3+} in a local tetragonal CEF surrounding where Γ_6 doublet ($|\mp 1/2\rangle$) was proposed to be the ground state [26,39]. One may note that the saturated M value begins to decrease gradually for $x \geqslant 0.8$ and reaches a value of $0.85\,\mu_B$ for $x = 1$. We ascribe this decrease of saturation moment to the crystal field effects. Figure 4(b) shows the derivative of magnetization with respect to magnetic field. Accordingly, the relationship between the derived FM saturation field and Ru substitution level is mapped in the inset of fig. 4(b). It is clear that the extrapolated FM saturation field decreases monotonously from 4.29 tesla ($x = 0.5$) to 0.85 tesla ($x = 1$). This is consistent with the susceptibility upturn shown in fig. 3 that the FM coupling between Ce^{3+} ions is enhanced by Ru substitution significantly.

Figure 5 shows the results of low-temperature specific-heat measurements for $CeFe_{1-x}Ru_xAsO$ ($x = 0.5$, 0.8, 1.0) in a fixed magnetic field (0 T, 8 T). For $x = 0.5$ at 0 T, the specific heat increases rapidly upon cooling. When a static magnetic field of 8 T is applied to the sample, the upturn at low temperature is suppressed, followed by the emergence of a broad peak at around 3.8 K. This indicates that the specific-heat upturn in zero field should be mostly contributed by magnetic instability rather than Kondo screening effects. For the samples with $x = 0.8$ and 1.0, the broad peaks of 8 T shift to 4.3 K and 5.4 K, respectively. This suggest that the FM correlation is strengthened by

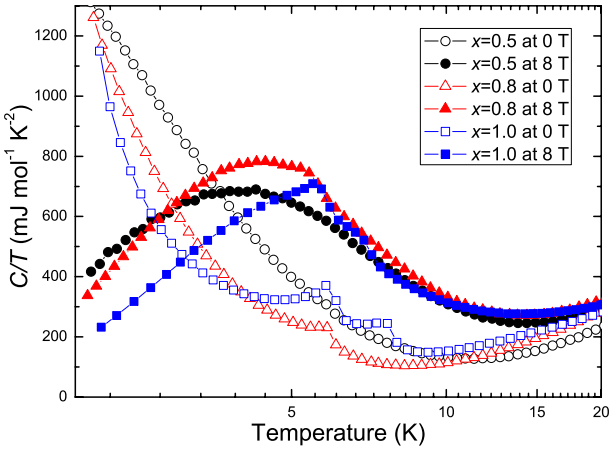

Fig. 5: (Color online) Temperature dependence of specific heat for $CeFe_{1-x}Ru_xAsO$ ($x = 0.5$, 0.8, 1.0) under a magnetic field of 0 T and 8 T, respectively.

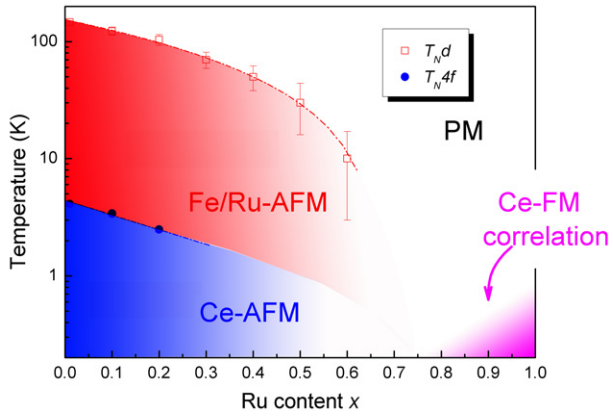

Fig. 6: (Color online) Electronic phase diagram of $CeFe_{1-x}Ru_xAsO$ ($0 \leqslant x \leqslant 1$). $T_N d$ and $T_N f$ represent the respective Néel temperatures of d and f electrons. $T_N d$ is derived from the resistivity anomaly using the method proposed by Klauss *et al.* [40], and $T_N 4f$ is denoted by the peak in the susceptibility.

Ru substitution, which is consistent with both M-T and M-H measurement. It is noted that there is one (two) small peak on the zero-field curve of $x = 0.8$ ($x = 1$). We ascribe this phenomenon to trace the amount of Ce_2O_3 impurity which undergoes AFM transition between 5.7 K to 8.6 K [41].

We summarize the experimental results by suggesting the electronic phase diagram shown in fig. 6. As far as the d electrons are concerned, the phase diagram can be divided into two parts: For $x \leqslant 0.6$, the d electrons show AFM spin density wave at low temperature, while for $x \geqslant 0.7$, the d electrons exhibit Pauli PM behavior over the entire temperature range. It is well known that a similar AFM-PM transition followed by superconductivity is observed in phosphorus-doped "1111" and "122" systems, which is ascribed to quantum critical behavior

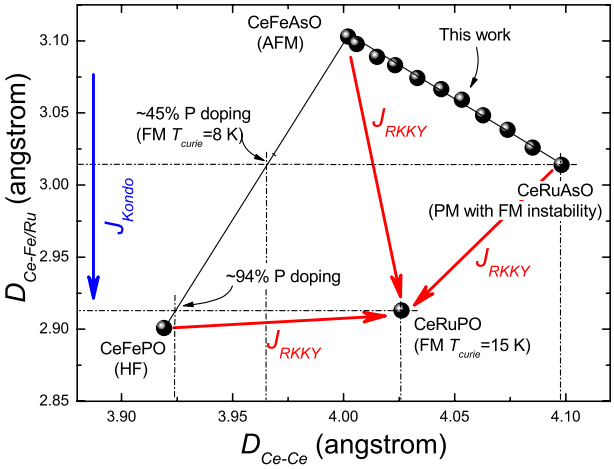

Fig. 7: (Color online) Schematic diagram of the quaternary compounds $CeMXO$(M = Fe, Ru; X = P, As). The red and blue arrows indicate the direction of increasing J_{RKKY} and J_{Kondo}, respectively.

induced by the enhanced itinerancy of d electrons [15,20]. Similarly, the enhanced itinerancy of d electrons is also observed in Ru-doped "122" phases [23,24], which may explain the origin of the resulting superconductivity [19]. In Ru-doped "1111" phases however, no superconductivity above 2 K has been reported so far. Meanwhile, nearly twice as much Ru substitution as in "122" phases is required to suppress the AFM order of d electrons. This may suggest that Ru substitution in "1111" compounds does not enhance the itinerancy of d orbitals as much as it does in the "122" system. Nevertheless, more direct evidence is required to clarify this question. As for the $4f$ electrons, the $T_N f$ gradually decreases from 4.1 K ($x = 0$) to 2.6 K ($x = 0.2$). Higher doping leads to a further suppression of the $T_N f$ that cannot be observed directly down to 2 K. At the same time, The FM correlation is gradually strengthened by Ru substitution, suggesting the strong d-f coupling in the $CeFe_{1-x}Ru_xAsO$ system.

To clarify the relationship between the crystal structure and the ground state of $4f$ orbital, we map the four quaternary compounds $CeMXO$(M = Fe, Ru; X = P, As) in fig. 7 according to their different $D_{\text{Ce-Fe/Ru}}$ and $D_{\text{Ce-Ce}}$. It is now known that the d-f coupling determines the properties of Ce-based "1111" compounds, which is very different from other lanthanide analog. The ground state of $4f$ electrons is mainly controlled by two kinds of interactions, including i) the direct Kondo coupling (J_{Kondo}) between localized $4f$ electrons and itinerate d electrons, and ii) the indirect RKKY coupling (J_{RKKY}) between two separate Ce atoms. While J_{Kondo} is negatively correlated with $D_{\text{Ce-Fe/Ru}}$ [29], the dependence on $D_{\text{Ce-Ce}}$ of J_{RKKY} is a Friedel oscillation following the equation: $J_{RKKY}(r) \sim -J_{Kondo}^2 N_F \frac{\cos 2k_F r}{k_F r}$, where N_F is the density of states (DOS) at the Fermi level, k_F is the Fermi momentum and r is the distance between two Ce

atoms. In the case of $CeFeAs_{1-x}P_xO$, the shrinkage of $D_{\text{Ce-Fe}}$ is 0.202 Å, which greatly strengthens J_{Kondo} and finally induces heavy-fermion behavior for $x \geqslant 0.95$ [29]. In the case of $CeFe_{1-x}Ru_xAs$, on the other hand, the total shrinkage of $D_{\text{Ce-Fe/Ru}}$ is 0.089 Å, equivalent to that of $\sim 45\%$ P substitution in $CeFeAs_{1-x}P_xO$. This quantitative analysis is consistent with the similarity of the two phase diagrams, so that the role of the end member CeRuAsO in the $CeFe_{1-x}Ru_xAs$ system is rather similar to that of the $CeFeAs_{0.55}P_{0.45}O$ in $CeFeAs_{1-x}P_xO$, where the FM state has just been stabilized. In addition, the $D_{\text{Ce-Ru}}$ value in CeRuPO is 2.913 Å, equivalent to that of $\sim 94\%$ P doping in $CeFeAs_{1-x}P_xO$ where the heavy-fermion behavior is about to dominate. This is also consistent with the incomplete Kondo screening of the $4f$ local moments in CeRuPO [27].

As for the J_{RKKY} which is dependent on both J_{Kondo} and $D_{\text{Ce-Ce}}$, the situation is more complex. However, we can still estimate the trend of J_{RKKY} by comparing the FM ordering temperature. As is shown in fig. 7, the Curie temperature of CeRuPO and $CeFeAs_{0.55}P_{0.45}O$ are 15 K and 8 K respectively [27,29]. Thus considering the PM state with strong FM instability in CeRuAsO, it is reasonable to believe there should be a maximum of J_{RKKY} hovering around CeRuPO. This speculation is consistent with the heavy-fermion behavior of CeFePO, where J_{Kondo} rules the ground state of $4f$ electrons. Meanwhile, the high-pressure experiment in CeFePO [42] can also be understood easily, that the Kondo screening of Ce $4f$ moments is further stabilized by the pressure-induced shrinkage of both $D_{\text{Ce-Fe/Ru}}$ and $D_{\text{Ce-Ce}}$.

Concluding remarks. – To conclude, our experiment results of $CeFe_{1-x}Ru_xAsO$ $(0 \leqslant x \leqslant 1)$ show that strong FM instability emerges after AFM states of both d and $4f$ electrons are killed by Ru substitution. Combined with structural refinement data and other published works, we provide a picture of the relationship between the ground state of $4f$ electrons and the crystal structure in $CeMXO(M = \text{Fe, Ru};\ X = \text{P, As})$ compounds. The combined effects of J_{Kondo} and J_{RKKY} determine the ground state of $4f$ electrons, ranging from localized AFM ordering to an FM Kondo lattice and an itinerant heavy-fermion metal. In addition, this also leads to a prediction that heavy-fermion behavior may be introduced into both CeRuAsO and CeRuPO by applying an adequate physical or chemical pressure.

* * *

This work is supported by an Australian Research Council Discovery Project (DP120100095), the National Basic Research Program of China (No. 2010CB923003) and the National Science Foundation of China (No. 10934005).

REFERENCES

[1] Kamihara Y. *et al.*, *J. Am. Chem. Soc.*, **130** (2008) 3296.
[2] Ren Z. A. *et al.*, *EPL*, **83** (2008) 17002.
[3] Prakash J. *et al.*, *J. Phys.: Condens. Matter*, **21** (2009) 175705.
[4] Wen H. H. *et al.*, *EPL*, **82** (2008) 17009.
[5] Chen X. H. *et al.*, *Nature*, **453** (2008) 761.
[6] Chen G. F. *et al.*, *Phys. Rev. Lett.*, **100** (2008) 247002.
[7] Ren Z. A. *et al.*, *EPL*, **82** (2008) 57002.
[8] Ren Z. A. *et al.*, *Mater. Res. Innov.*, **12** (2008) 105.
[9] Wang C. *et al.*, *EPL*, **83** (2008) 67006.
[10] Li L. J. *et al.*, *Phys. Rev. B*, **78** (2008) 132506.
[11] Wang C. *et al.*, *EPL*, **86** (2009) 47002.
[12] Li Y. K. *et al.*, *Physica C*, **470** (2010) S493.
[13] Pallecchi I. *et al.*, *Phys. Rev. B*, **84** (2011) 134524.
[14] Ren Z. *et al.*, *Phys. Rev. Lett.*, **102** (2009) 137002.
[15] Jiang S. *et al.*, *J. Phys.: Condens. Matter*, **21** (2009) 382203.
[16] Shi H. L. *et al.*, *J. Phys.: Condens. Matter*, **22** (2010) 125702.
[17] Jiao W. H. *et al.*, *EPL*, **95** (2011) 67007.
[18] Schnelle W. *et al.*, *Phys. Rev. B*, **79** (2009) 214516.
[19] Sharma S. *et al.*, *Phys. Rev. B*, **81** (2010) 174512.
[20] Dao J. H. *et al.*, *Proc. Natl. Acad. Sci. U.S.A.*, **106** (2009) 4118.
[21] Si Q. and Abrahams E., *Phys. Rev. Lett.*, **101** (2008) 076401.
[22] Si Q. *et al.*, *New J. Phys.*, **11** (2009) 045001.
[23] Brouet V. *et al.*, *Phys. Rev. Lett.*, **105** (2010) 087001.
[24] Kim M. G. *et al.*, *Phys. Rev. B*, **83** (2011) 054514.
[25] Zhao J. *et al.*, *Nat. Mater.*, **7** (2008) 953.
[26] Brüning E. M. *et al.*, *Phys. Rev. Lett.*, **101** (2008) 117206.
[27] Krellner C. *et al.*, *Phys. Rev. B*, **76** (2007) 104418.
[28] Chen G. F. *et al.*, *Chin. Phys. Lett.*, **25** (2008) 2235.
[29] Luo Y. K. *et al.*, *Phys. Rev. B*, **81** (2010) 134422.
[30] M. A. McGuire M. A. *et al.*, *J. Solid State Chem.*, **182** (2009) 2326.
[31] McCusker L. B. *et al.*, *J. Appl. Cryst.*, **32** (1999) 36.
[32] Bérardan D. *et al.*, *Phys. Rev. B*, **81** (2010) 094506.
[33] Chen Y. L. *et al.*, *J. Am. Chem. Soc.*, **131** (2009) 10338.
[34] Maroni B. *et al.*, *Phys. Rev. B*, **82** (2010) 104503.
[35] Zimmer B. I. *et al.*, *J. Alloys Compd.*, **229** (1995) 238.
[36] Dai J. H. *et al.*, *EPL*, **87** (2009) 17005.
[37] Tropeano M. *et al.*, *Phys. Rev. B*, **81** (2010) 184504.
[38] Bonfà P. *et al.*, *Phys. Rev. B*, **85** (2012) 054518.
[39] Chi S. *et al.*, *Phys. Rev. Lett.*, **101** (2008) 217002.
[40] Klauss H.-H. *et al.*, *Phys. Rev. Lett.*, **101** (2008) 077005.
[41] Huntelaar M. E. *et al.*, *J. Chem. Thermodyn.*, **32** (2000) 465.
[42] Zocco D. A. *et al.*, *Phys. Rev. B*, **83** (2011) 094528.